J Mater Sci (2011) 46:3330–3336
DOI 10.1007/s10853-010-5220-y

Preparation and characterization of zirconia and mixed zirconia/titania in ionic liquids

Hala K. Farag · Khaled H. Hegab · S. Zein El Abedin

Received: 8 August 2010 / Accepted: 24 December 2010 / Published online: 8 January 2011

Abstract Zirconia and mixed zirconia/titania were synthesized in two different ionic liquids, namely, 1-butyl-1-methylpyrrolidinium bis(trifluoromethylsulfonyl) amide ([BMP]TFSA) and 1-ethyl-3-methylimidazolium bis(trifluoromethylsulfonyl) amide ([EMIm]TFSA) using sol–gel methods. The synthesized oxides were characterized by means of X-ray diffraction, scanning electron microscopy with energy dispersive X-ray (SEM-EDX)), thermogravimetric and differential thermal analyses (TGA–DTA). The results show that the as-synthesized ZrO_2 powders obtained either in [BMP]TFSA or in [EMIm]TFSA show amorphous behaviour, and calcination at 500 °C yields t-ZrO_2 which is subject to further phase transformation to m-ZrO_2 at 1000 °C. The type of the ionic liquid influences the morphology of the synthesized zirconia as the sample obtained from [BMP]TFSA showed a porous morphology with very fine particles in the nanometer regime, whereas micro-rods were obtained from [EMIm]TFSA. ZrO_2-TiO_2 nanorods with an average diameter of about 100 nm were synthesized in [EMIm]TFSA. The presence of zirconia in the mixed oxides stabilizes the anatase phase and elevates the temperature at which the phase transformation to rutile occurs.

H. K. Farag (✉) · K. H. Hegab
Inorganic Chemistry Department, National Research Centre, El Tahrir St., Dokki, Cairo, Egypt
e-mail: msherif888@yahoo.com

S. Zein El Abedin
Electrochemistry and Corrosion Laboratory, National Research Centre, Dokki, Cairo, Egypt

Present Address:
K. H. Hegab
Chemistry Department, Faculty of Science, Gazan University, Gazan, Saudi Arabia

Present Address:
S. Zein El Abedin
Institute of Particle Technology, Clausthal University of Technology, Clausthal-Zellerfeld 38678, Germany
e-mail: sherif.zein@tu-clausthal.de

Introduction

Zirconia (ZrO_2) has gained extensive attention because of its diverse applications in, e.g., fuel cells [1], gas sensors [2] and catalysis [3]. ZrO_2 has superior physical properties, such as high thermal and chemical stability, low electrical conductivity, high dielectric constant and biocompatibility. Due to its high oxygen ion conductivity, zirconia is considered as a potential solid electrolyte in oxygen sensors and solid oxide fuel cells [4, 5]. It is categorized as a wide band gab semiconductor and it becomes more conductive with increasing temperatures. Zirconium oxide is known to be crystallized into three different structures depending on the annealing temperatures (T): monoclinic ($T < 1170$ °C), tetragonal ($T = 1170$–2370 °C) and cubic ($T > 2370$ °C). Tetragonal and cubic structures are those relevant for technological applications, based on their oxygen conductivity, in solid oxide fuel cells, sensors and in catalysis. The cubic or tetragonal forms can be stabilized at room temperature by the addition of CaO and Y_2O_3 [6]. Stabilization of the tetragonal ZrO_2 by quite low concentrations of either Sm_2O_3 or Tb_2O_3 was reported [7].

The synthesis of zirconia powders was described using various routes such as sol–gel [8, 9], co-precipitation [10, 11], hydrothermal process [12, 13], gas phase synthesis and microemulsion methods [14–16]. Sol–gel is a commonly used method for the synthesis of oxides involving the formation of an amorphous gel from a precursor solution.

One of the advantages of the sol–gel route is its potential for fabrication of solid-state inorganic materials in a variety of useful forms.

Ionic liquids with their unconventional physical properties, such as negligible vapour pressure, high thermal stability up to 300 °C, non-flammability, high ionic conductivity and excellent ability to dissolve inorganics and organics, are considered as potential solvents or co-solvents in sol–gel processing. Ionic liquids with different cation/anion combinations have the potential to act as multifunctional solvents, templates, stabilizers and crystal growth modifiers [17]. Generally, ionic liquids are more powerful than surfactants which are widely employed as templates since the same ionic liquid can lead to different structures when different precursors are used [18]. Quite recently, Zhang et al. [18] could tune the nanostructures of spheres and hollow spheres of ZnO during a solvothermal reaction using ionic liquids as soft templates. Antonietti and Smarsly [19, 20] reported on the synthesis of crystalline TiO_2 nanoparticles in ionic liquids by hydrolysis of titanium tetrachloride at 80 °C. Farag et al. [21, 22] demonstrated the high potential of air and water stable ionic liquids for the synthesis of nanostructured alumina as well as a high surface area mixed alumina–titania. The sol–gel synthesis of titania, anatase and rutile by hydrolysis of $TiCl_4$ in different ionic liquids was also reported [23]. Furthermore, synthesis of vanadia powders in two different ionic liquids, [BMP]TFSA and [EMIm]TFSA, was described [24]. In order to get more information of the use of ionic liquids in sol–gel synthesis of inorganic or organically modified materials we refer to a recently published review article [25].

In this article, sol–gel methods were employed for the synthesis of zirconia and mixed zirconia–titania in the ionic liquids [BMP]TFSA and [EMIm]TFSA using zirconium butoxide and titanium isopropoxide precursors. Two ionic liquids with the same anion and different cations were employed to show the effect of the cation type on the sol–gel growth of zirconia. The phase transformation obtained by calcination of the synthesized oxides at variable temperatures was investigated by X-ray diffraction (XRD), thermogravimetric and differential thermal analyses (TGA–DTA). The surface morphology of the obtained oxides was studied by a high-resolution scanning electron microscope (SEM).

Experimental

Materials

The ionic liquids 1-butyl-1-methylpyrrolidinium bis(trifluoromethylsulfonyl) amide ([BMP]TFSA) and 1-ethyl-3-methylimidazolium bis(trifluoromethylsulfonyl) amide ([EMIm]TFSA) were purchased from Merck KGaA (EMD) in ultrapure quality. Zirconium butoxide ($Zr(OBu)_4$) (Aldrich, 80 wt% in butanol) and titanium isopropoxide ($Ti(OPr\text{-}i)_4$) (Aldrich 99.99%) were used without further purification as precursors for synthesis of zirconia and titania, respectively. Bi-distilled water was used for hydrolysis the precursor solutions. Acetone (Alfa 99.5%) was used for refluxing the obtained oxides. Preparations of solutions were carried out in an argon-filled glove box with water and oxygen contents below 2 ppm (OMNI-LAB from Vacuum-Atmospheres).

Synthesis of zirconia and mixed zirconia–titania

The zirconia was synthesized in [BMP]TFSA and in [EMIm]TFSA. A solution of 1 M $Zr(OBu)_4$ was prepared and then hydrolysed by dropwise addition of appropriate amount of water. An emulsion was formed and then aged at 90 °C for about 12 h to form a gel, the system was kept stirring. Afterwards, approximately a 2-fold volume of acetone was added into the reaction system and stirring maintained with refluxing at 50 °C for about 12 h. Then the mixture was centrifuged to reclaim the hydrolysis product. Finally, the hydrolysis product was left to dry in dry air for about 24 h, before calcinations. Zirconia–titania was synthesized by co-hydrolysis of a mixture of 1 M $Zr(OBu)_4$ and 1 M $Ti(OPr\text{-}i)_4$ in [EMIm]TFSA. The synthesized samples were calcined in a muffle oven at the desired temperature for 2 h and were cooled down to the ambient temperature in the oven.

Characterization

The morphology of the as-prepared zirconia and mixed zirconia–titania was investigated by means of a high-resolution field emission scanning electron microscope (Carl Zeiss DSM 982 Gemini). The phase compositions of the as-prepared and calcined samples were analysed by X-ray diffractogram (XRD) using a Siemens D-5000 diffractometer with CoKα radiation. Thermal gravimetric and differential thermal analyses (TGA–DTA) were carried out by a NETZSCH STA 409 PC thermal analyzer at a heating rate of 10 °C/min starting from room temperature up to 1000 °C in air.

Results and discussion

Synthesis of zirconia in [BMP]TFSA

The XRD patterns of as-synthesized and calcined zirconia samples prepared in the ionic liquid [BMP]TFSA are

shown in Fig. 1. The as-synthesized zirconia was calcined at 250, 500, 750, and 1000 °C to investigate the structural transformations of zirconia. As manifested in Fig. 1, the as-synthesized zirconia shows amorhous behaviour, since no diffraction peaks are recorded. This might indicate that the synthesized zirconia contains very fine crystallites to the extent that no diffraction peaks could be recorded within the resolution of our XRD device. Calcination of the synthesized zirconia sample at 250 °C leads to very slight improvement of the crystallization of zirconia as a very wide peak was recorded where tetragonal zirconia (t-ZrO_2) has its main peaks. At 500 °C, a well-crystallized tetragonal zirconia was obtained. All diffraction peaks can be perfectly indexed to the data available in the JPCD 17-0923 diffraction file. The broadening of the diffraction peaks indicates the presence of very fine particles. The tetragonal structure shows some thermal stability at 750 °C, although a very weak peak for the monoclinic structure (m-ZrO_2) is also recorded. Following calcination at 1000 °C the synthesized zirconia shows a complete transformation to the monoclinic structure (JPCD 36-0420). Generally, the transformation of t-ZrO_2 to m-ZrO_2 was reported to occur at temperatures less than 800 °C [26–28]. Thus, the zirconia prepared in [BMP]TFSA shows a high thermal stability of its tetragonal phase as the transformation to monoclinic occurs at 1000 °C. To investigate the morphology of the synthesized ZrO_2 powder a high-resolution field emission scanning electron microscope was used. The SEM micrograph of Fig. 2 shows the morphology of a zirconia sample obtained in [BMP]TFSA and calcined at

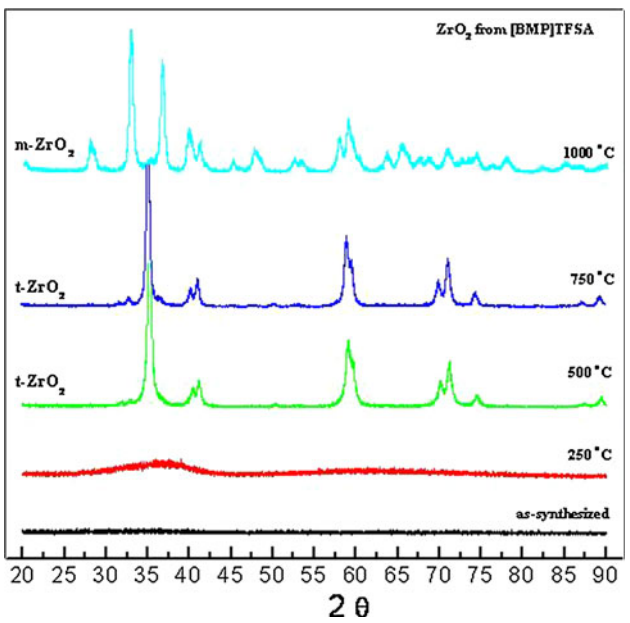

Fig. 1 XRD patterns of as-synthesized zirconia prepared in [BMP]TFSA containing 1 M $Zr(OBu)_4$, without and with calcinations at different temperatures

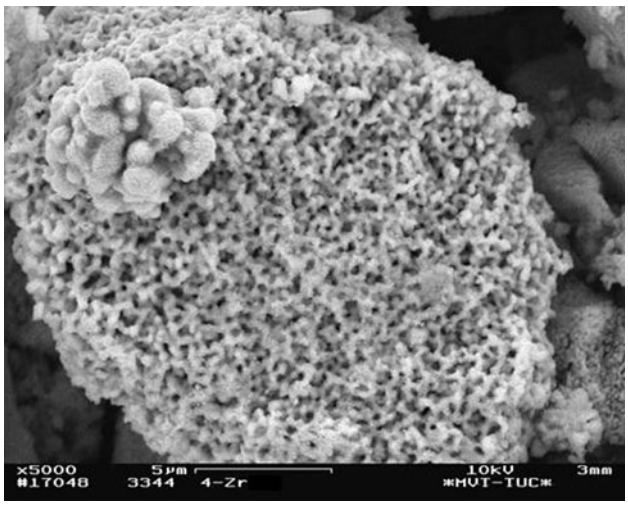

Fig. 2 SEM micrograph of a zirconia sample obtained in [BMP]TFSA and calcined at 250 °C

250 °C for 2 h. As can be seen, the sample shows a porous morphology with very fine particles of sizes in the nanometer regime.

Further structural transformations of the as-synthesized zirconia with heat treatment were studied using TGA–DTA analyses. Typical TGA–DTA curves of the as-synthesized zirconia are shown in Fig. 3. The TG curve shows a gradual mass loss of about 20% in the temperature range of 35–300 °C and then a mass loss of about 10% in the temperature range of 300–450 °C. The first mass loss is due to the evaporation of physically adsorbed water as well as the residual organic solvent. The mass loss in the temperature range 300–450 °C is attributed to the decomposition of the ionic liquid residues. Visually, the as-prepared

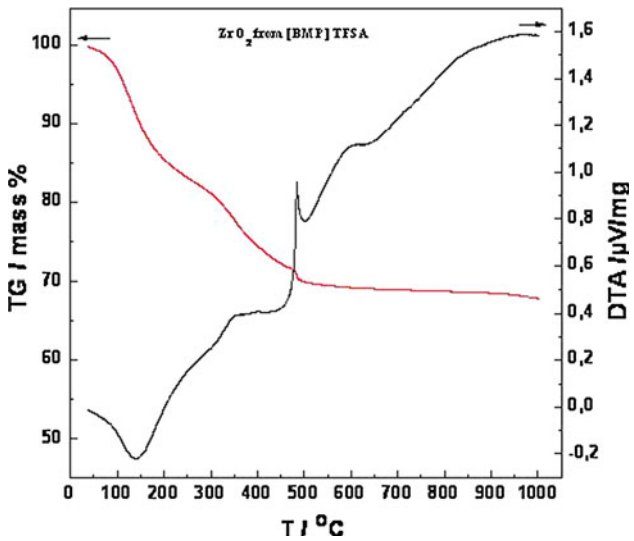

Fig. 3 DTA–TGA curves of the as-synthesized zirconia sample obtained in [BMP]TFSA

samples appear grey in colour in the temperature range of 300–450 °C due to the presence of char residues, as a result of the thermal decomposition of the remaining ionic liquid, which oxidize to volatile products. No significant mass loss was observed after 500 °C.

The DTA curve exhibits some endothermic and exothermic processes. The initial broad endotherm observed at about 140 °C is correlated to the evolution of the adsorbed water. The DTA curve displays a sharp exothermic peak at 482 °C followed by an exothermic rise up to 900 °C with an exothermic hump at 600 °C. The sharp exothermic peak might be attributed to the transformation of amorphous to tetragonal crystalline structure. This can be evidenced by the XRD results of Fig. 1 as at 500 °C a well-crystallized t-ZrO_2 is obtained. The subsequent exothermic rise in the DTA curve can be ascribed to the crystallization and starting of the transformation of t-ZrO_2 to m-ZrO_2.

Synthesis of zirconia in [EMIm]TFSA

Figure 4 shows the XRD patterns of as-synthesized and calcined zirconia samples obtained in the ionic liquid [EMIm]TFSA. As displayed in Fig. 4, the as-synthesized ZrO_2 exhibits poor crystallization as only a very broad peak was recorded. After calcination of the as-synthesized sample at 250 °C, no significant improvement in the crystallization was observed. At 500 °C, well-crystallized t-ZrO_2 was obtained. At 750 °C, the tetragonal phase remained dominant, but the characteristic peaks for the monoclinic phase began to emerge indicating the presence of some content of this crystalline phase. A transformation of t-ZrO_2 to m-ZrO_2 was observed at 1000 °C. However, the transformation was not complete as some traces of t-ZrO_2 were also recorded. The SEM micrographs of Fig. 5 show the morphology of the ZrO_2 powder prepared in [EMIm]TFSA. Interestingly, the obtained zirconia exhibits a fully different morphology from that of the zirconia obtained in [BMP]TFSA. As seen in Fig. 5 micro-rods are obtained with diameters ranging from 0.4 to 1 μm and lengths from 4 to 25 μm. Therefore, it can be concluded that the cation type of the employed ionic liquids influences the sol gel growth of zirconia which, in turn, leads to modified morphologies. The influence of the type of ionic liquid on the sol–gel growth of alumina [21] and vanadia [24] was reported. Quite recently Endres and Atkin [29, 30] showed that ionic liquids are adsorbed on solid surfaces and this adsorption is that strong that several layers of ionic liquids are formed on the surface. Both [BMP]TFSA and [EMIm]TFSA are adsorbed differently: [BMP]TFSA is roughly four times more strongly adsorbed than [EMIm]TFSA [29]. This is not surprising as the positive charge is localized in the case of $[BMP]^+$ and delocalized for $[EMIm]^+$ which, in turn, leads to higher electrostatic interactions between the surface and $[BMP]^+$. Based on these data it can be assumed that the increased strength of adsorption of [BMP]TFSA compared to [EMIm]TFSA might lead to the difference in morphology of the zirconia obtained in both liquids. The strong adsorption of [BMP]TFSA to the surface of the growing nuclei hinders their further growth, leading to very fine zirconia particles with sizes in the nanometer regime, see Fig. 2. However, due to the weak adsorption of [EMIm]TFSA to the nucleation sites the nuclei aggregate and self-assemble into rod-like structure, Fig. 5. No significant influence was found for the cation type on the phase behaviour of the zirconia samples. Zirconia obtained in both liquids shows amorphous behaviour which is subject to transformations to t-ZrO_2 and m-ZrO_2 at 500 and 1000 °C, respectively.

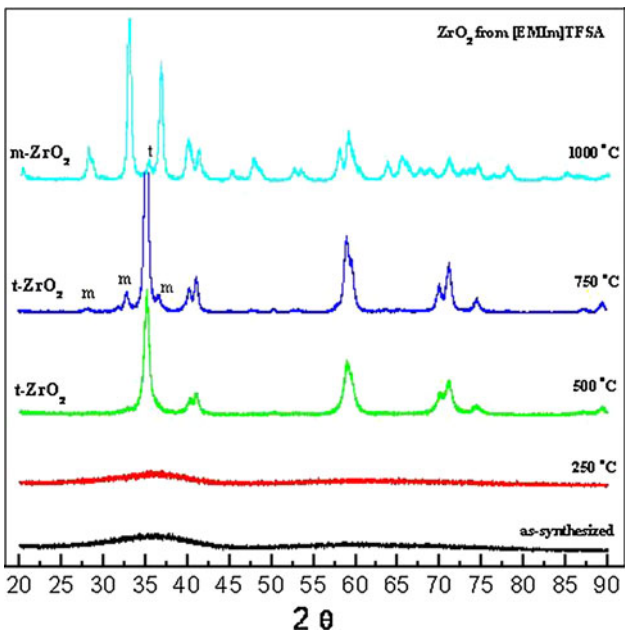

Fig. 4 XRD patterns of as-synthesized zirconia prepared in [EMIm]TFSA containing 1 M $Zr(OBu)_4$, without and with calcinations at different temperatures

The TGA–DTA curves of the synthesized zirconia in [EMIm]TFSA are displayed in Fig. 6. The TGA curve displays a rapid decrease in mass (about 15%) in the temperature range of 100–160 °C, and then the mass exponentially decreases up to about 480 °C. The TGA curve does not show any mass loss beyond 500 °C. The first mass loss can be ascribed to the removal of adsorbed water and the remaining organic solvent. As a result, an endothermic peak was observed in the DTA curve at 160 °C. The second mass loss (the exponential one) might be correlated with the combustion of the ionic liquid residues. No defined exothermic peak for such combustion was observed in the DTA curve. A small exothermic shoulder was recorded at about 500 °C, followed by an exothermic rise signifying the crystallization of ZrO_2.

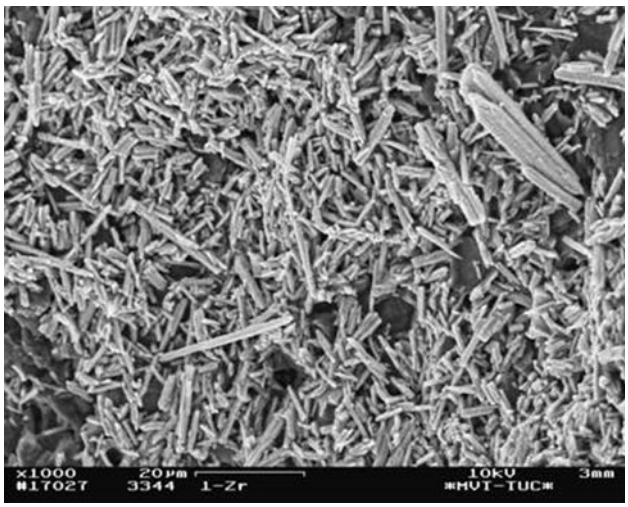

Fig. 5 SEM micrograph of a zirconia sample obtained in [EMIm]TFSA and calcined at 250 °C

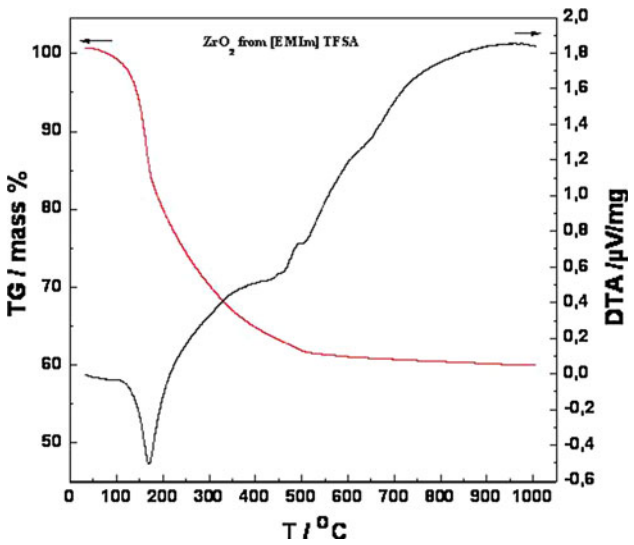

Fig. 6 DTA–TGA curves of the as-synthesized zirconia sample obtained in [EMIm]TFSA

The aforementioned results reflect the high potential of ionic liquids in the sol gel synthesis of nanostructured materials. As shown, the type of the ionic liquid influences the morphology of the synthesized zirconia as the sample obtained from [BMP]TFSA showed a porous morphology with very fine particles in the nanometer regime, whereas micro-rods were obtained from [EMIm]TFSA. In addition to providing environmentally benign conditions the use of ionic liquids in the sol–gel synthesis of crystalline materials can lead to tune the size and shape of crystals. Furthermore, ionic liquids with different cation/anion combinations have the potential to act as multifunctional solvents; templates, stabilizers and crystal growth modifiers. Thus, the use of additives as shape directing/templating agents can be eliminated by employing ionic liquids.

Synthesis of zirconia–titania composite

As known, both ZrO_2 and TiO_2 single oxides exhibit excellent catalytic properties for various reactions, and both of them are n-type semiconductors. Mixed zirconia–titania oxides have properties superior to those of single-metal oxides, as they exhibit high surface area, powerful surface acid–base properties, high thermal stability and strong mechanical strength [31–33]. The mixed oxides not only take advantages of both TiO_2 (active catalyst and support) and ZrO_2 (acid–base properties) but also extend their applications through the generation of new catalytic sites due to a strong interaction between them [33]. Therefore, it seemed of interest to synthesize mixed ZrO_2/TiO_2.

Zirconia–titania powders with a molar ratio of 1:1 were sol gel synthesized by co-hydrolysis of equal molar concentrations of $Zr(OBu)_4$ and $Ti(OPr\text{-}i)_4$ in [EMIm]TFSA. The as-synthesized composite was calcined at different temperatures to investigate the crystalline phases formed during calcinations. Figure 7 shows the XRD patterns of as-synthesized and calcined ZrO_2–TiO_2 samples. As shown, the as-synthesized sample is amorphous and the crystallinity does not significantly improve on calcination at 250 °C. However, at 500 °C pronounced diffraction peaks characteristic of monoclinic ZrO_2 (JPCD 36-0420) and anatase TiO_2 (JCPD 21-1272) were observed. Furthermore, the main diffraction peak of $ZrTiO_4$ was recorded (JCPD 34-0415). The existence of $ZrTiO_4$ was reported for ZrO_2-TiO_2 composites calcined at 700 °C, and its content increases as the zirconia content increases [34]. Interestingly, the metastable tetragonal phase of zirconia was not detected in the mixed ZrO_2–TiO_2 unlike in the

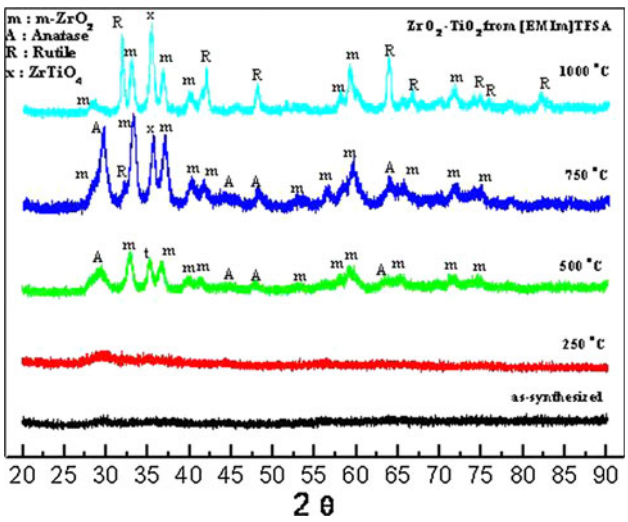

Fig. 7 XRD patterns of zirconia–titania samples prepared in [EMIm]TFSA containing 1 M $Zr(OBu)_4$ and 1 M $Ti(OPr\text{-}i)_4$, without and with calcinations at different temperatures

single ZrO_2. Moreover, the monoclinc phase emerges at 500 °C whereas; it appears at 1000 °C in the single oxide. This signifies that the presence of titania enhances the formation of m-ZrO_2 at low temperatures. At 750 °C, no new phases were observed and the anatase phase was still thermally stable. Usually, the anatase phase transforms to rutile at 500–600 °C [35]. Therefore, it can be stated that the presence of zirconia stabilizes the anatase phase and rises the temperature at which the phase transformation to rutile takes place. This might lead to overcome the drawbacks of using titania single oxide as a catalyst at high temperatures owing to the poor thermal stability of its anatase phase (the catalytically active phase). The anatase completely transformed to rutile at 1000 °C (JCPD 34-0180). As known, the metastable anatase phase transforms to rutile when the thermal energy is high enough to overcome the nucleation energy. Generally, an increase in the crystallite sizes promotes the transformation due to the small nucleation barrier as a result of the increase in microstructural defects. A practical pathway to control the temperature of the anatase–rutile phase transition is doping of TiO_2 with other metal oxides. It was postulated that the additives that provide nucleation sites (e.g. by preferential segregation) enhance the phase transition [36], whereas the additives that are of the same valence and occupy interstitial sites retard the transformation [37]. It was also assumed that additives which reduce particle contact can retard the anatase–rutile transformation [38]. A critical size mechanism was also suggested for the anatase–rutile transformation in pure TiO_2 and doped-TiO_2. Morries et al. [39] showed that the mechanism for the phase transformation is related to attaining a critical particle size of about 45 nm. However, Hirano et al. [40] found that the transformation occurs when the crystallite size reaches approximately 70 nm by heating in both cases for pure TiO_2- and ZrO_2-doped TiO_2. Regardless the value of the critical particle size it is well satisfactory that the temperature of anatase–rutile transition is strongly dependent on the crystallite size. As the crystallite size of the mixed ZrO_2–TiO_2 is fairly reduced, heating at higher temperatures is necessary to reach the critical crystallite size for the anatase–rutile phase transformation. Furthermore, the presence of zirconia retards the mass transport to attain the critical particle size. This might be a possible explanation for the high thermal stability of the anatase phase in the presence of zirconia.

The SEM micrographs of Fig. 8 present the morphology of a ZrO_2–TiO_2 sample calcined at 250 °C. The SEM micrograph of Fig. 8a shows ZrO_2–TiO_2 bundles which composed of many packed, ordered nanorods. The high-resolution SEM micrograph of Fig. 8b shows the arrangement of ordered nanorods with an average diameter of about 100 nm.

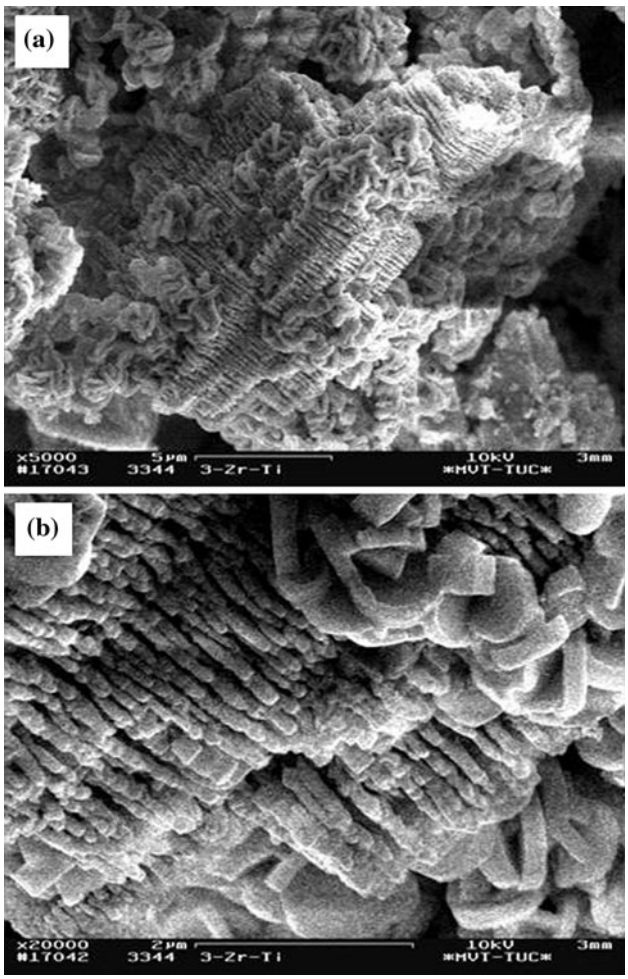

Fig. 8 SEM micrographs of a zirconia–titania sample obtained in [EMIm]TFSA and calcined at 250 °C

Figure 9 presents the TGA–DTA curves of the as-synthesized ZrO_2–TiO_2 sample. Three weight loss processes can be identified in the TGA curve. The first weight loss (about 10%) was observed between 35 and 270 °C which can be correlated to the evaporation of adsorbed water and removal of organic impurities. The second weight loss (35%) was recorded in the temperature range of 270–450 °C which attributed to the thermal decomposition of the ionic liquid and alkoxides residues. The high temperature weight loss observed beyond 450 °C might be ascribed to the removal of the surface hydroxyls and/or evaporation of chemisorbed water. The DTA curve exhibits an exothermic peak at 140 °C and three exothermic peaks at 400, 480, and 730 °C with an exothermic rise from 880 to 1000 °C. The recorded enodothermic peak is attributed to the evaporation of adsorbed water. The first exothermic peak might be ascribed to the combustion of the remaining ionic liquid, and the second peak can be assigned to the crystallization of the amorphous sample (see Fig. 7). The broad exotherm is caused by the continued crystallization

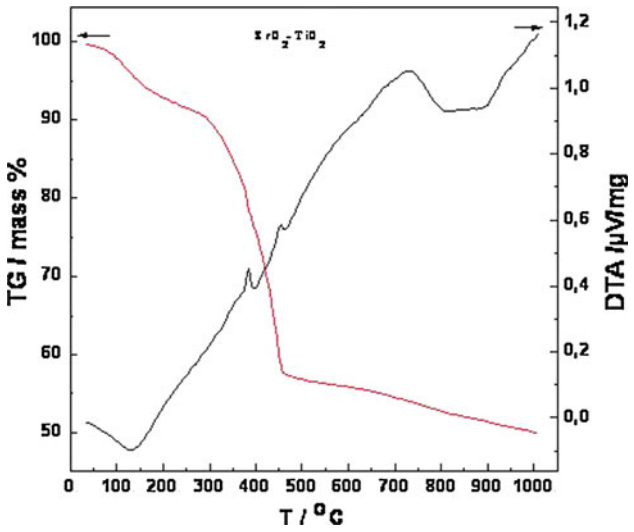

Fig. 9 DTA–TGA curves of the as-synthesized zirconia–titania sample obtained in [EMIm]TFSA

of the sample. The exothermic rise observed from 880 to 1000 °C might indicate the transformation of anatase to rutile.

Conclusions

Zirconia was sol gel synthesized in the ionic liquids [BMP]TFSA and [EMIm]TFSA. Furthermore, mixed zirconia–titania with a molar ratio 1:1 was obtained in the ionic liquid [EMIm]TFSA using zirconium butoxide and titanium isopropoxide precursors. In both liquids, the as-synthesized ZrO_2 powders exhibit amorphous behaviour and calcination at 500 °C yields t-ZrO_2 which is subject to phase transformation to m-ZrO_2 at 1000 °C. The type of the ionic liquid influences the morphology of the synthesized zirconia. The sample obtained from [BMP]TFSA shows a porous morphology with very fine particles in the nanometer regime. Whereas micro-rods with diameters ranging from 0.4 to 1 µm and lengths from 4 to 25 µm were obtained using [EMIm]TFSA. ZrO_2-TiO_2 nanorods with an average diameter of about 100 nm were synthesized in [EMIm]TFSA. The presence of titania in the composite enhances the formation of m-ZrO_2 at low temperatures. Furthermore, zirconia stabilizes the anatase phase and elevates the temperature at which the phase transformation to rutile takes place, overcoming the drawbacks of employing titania single oxide as a catalyst at high temperatures.

Acknowledgement The authors would like to thank Prof. Dr. Frank Endres, Clausthal University of Technology, Germany, for generous help and fruitful discussions.

References

1. Park S, Vohs JM, Gorte RJ (2000) Nature 404:265
2. Ansori ZA, Karekar RN, Aiyer RC (1997) Thin Solid Films 305:330
3. Li YW, He DH, Cheng ZX, Su CL, Li JR, Zhu MJ (2001) Mol Catal A 175:267
4. Shukla S, Seal S (2005) Int Mater Rev 50:1
5. Liang J, Jiang X, Liu G, Deng Z, Zhuang J, Li F, Li Y (2003) Mater Res Bull 38:161
6. Chen S-Y, Lu H-Y (1988) J Mater Sci 23:1195. doi:10.1007/BF01154578
7. Cordova-Martinez W, De la Rosa-Cruz E, Diaz-Torres LA, Salas P, Montoya A, Avendano M, Rodriguez RA, Barbosa-Garcia O (2002) Opt Mater 20:263
8. Widoniak J, Eiden-Assmann S, Maret G (2005) Eur J Inorg Chem 15:3149
9. Kumazawa H, Inoue T, Sada E (1994) Chem Eng J 55:93
10. Haase F, Sauer F (1998) J Am Chem Soc 120:13503
11. Matusui K, Suzuki H, Ohagi M (1995) J Am Ceram Soc 78:146
12. Kumari L, Li WZ, Xu JM, Leblanc RM, Wang DZ, Li Y, Guo H, Zhang J (2009) Cryst Growth Des 9:3874
13. Kumari L, Du GH, Li WZ, Selva Vennila R, Saxena SK, Wang DZ (2009) Ceram Int 35:2401
14. Tai CY, Hsiao BY, Chiu HY (2007) Mater Lett 61:834
15. Tai CY, Lee MH, Wu YC (2001) Chem Eng Sci 56:2389
16. Tai CY, Hsiao BY (2005) Chem Eng Commun 192:1525
17. Farag HK (2011) Z Phys Chem 225:45
18. Zhang J, Wang J, Zhou S, Duan K, Feng B, Wenig J, Tang H, Wu P (2010) J Mater Chem 20:9798
19. Zhou Y, Antonietti M (2003) J Am Chem Soc 125:14960
20. Kapper H, Endres F, Djerdj I, Antonietti M, Smarsly BM, Maier J, Hu Y-S (2007) Small 3:1753
21. Farag HK, Endres F (2008) J Mater Chem 18:442
22. Farag HK, Al Zoubi M, Endres F (2009) J Mater Sci 44:122. doi:10.1007/s10853-008-3107-y
23. Al Zoubi M, Farag HK, Endres F (2008) Aust J Chem 61:704
24. Al Zoubi M, Farag HK, Endres F (2009) J Mater Sci 44:1363. doi:10.1007/s10853-008-3004-4
25. Vioux A, Viau L, Volland S, Bideau JL (2010) CR Chimie 13:242
26. Osendi MI, Moya JS, Serna CJ, Soria J (1985) J Am Ceram Soc 68:135
27. Garvie RC (1978) J Phys Chem 82:218
28. Shi JL, Lin ZX (1989) Solid State Ionics 32/33:544
29. Atkin R, Zein El Abedin S, Gasparotta LHS, Hayes R, Borisenko N, Endres F (2009) J Phys Chem 113:13266
30. Endres F, Höfft O, Borisenko N, Gasparotto LHS, Prowald A, Al-Salman R, Carstens T, Atkin R, Bound A, Zein El Abedin S (2010) Phys Chem Chem Phys 12:1724
31. Wu JC, Chung CC, Ay CL, Wang I (1984) J Catal 87:98
32. Wang I, Wu JC, Chung CC (1985) Appl Catal 16:89
33. Reddy BM, Khan A (2005) Catal Rev 47:257
34. Wan Y, Ma J, Zhou W, Zhu Y, Song X, Li H (2004) Appl Catal A 277:55
35. Jing LQ, Sun XJ, Cai WM, Xu ZL, Du YG, Fu HG (2003) J Phys Chem Solids 64:615
36. Chao HE, Yan YU, Xingfang HU, Larbol A (2003) J Eur Ceram Soc 23:1457
37. Arroya R, Corgoba G, Padilla J, Lara VH (2002) Mater Lett 54:397
38. Yoshinaka M, Hirota K, Yamaguchi O (1997) J Am Ceram Soc 80:2749
39. Reidy DJ, Holmes JD, Morris MA (2006) J Eur Ceram Soc 26:1527
40. Hirano M, Nakahara C, Ota K, Tanaike O, Inagaki M (2003) J Solid State Chem 170:39